Available online at www.sciencedirect.com
SCIENCE DIRECT®
Journal of Mechanics and Physics of solids
53 (2005) 123–142
JOURNAL OF THE MECHANICS AND PHYSICS OF SOLIDS
www.elsevier.com/locate/jmps

Mechanical properties of single-walled carbon nanotube bundles as bulk materials

J.Z. Liu[a], Q.-S. Zheng[a,*], L.-F. Wang[a], Q. Jiang[b,c]

[a]*Department of Engineering Mechanics, Tsinghua University, Yifu Technical Building, Beijing 100084, China*
[b]*College of Engineering, University of California, Riverside, CA 92521-0425, USA*
[c]*Institute of Mechanics and Sensor Technology, Central South University, Changsha 410083, China*

Received 16 September 2003; received in revised form 27 May 2004; accepted 5 June 2004

Abstract

Single-walled carbon nanotubes (SWNTs) in crystalline bundles may exhibit a transition in which the cross-sections of tubes turn from perfectly circular to hexagonal, depending upon the tube diameter and externally applied pressure, and this structural instability leads to an abrupt change in the bulk elastic properties of SWNT bundles. This paper presents a hybrid atom/continuum model to study the bulk elastic properties of SWNT bundles, and the predicted characteristics of this structural instability agree well with the experimental observations available in the literature. Linearized bulk elastic properties of SWNT bundles with respect to a stable configuration are transversely isotropic and hence can be characterized by five independent elastic moduli. A complete set of these five moduli is predicted for the first time. It is found that the deformability of tube cross-sections play a dominant role in characterizing the transverse moduli.

Keywords: Single-walled carbon nanotube bundle; A. buckling; B. anisotropic material; B. elastic material

*Corresponding author. Tel.: +86-106-277-1112; fax: +86-106-278-1824.
E-mail addresses: zhengqs@tsinghua.edu.cn (Q.-S. Zheng), qjiang@engr.ucr.edu (Q. Jiang).

0022-5096/$ - see front matter © 2004 Elsevier Ltd. All rights reserved.
doi:10.1016/j.jmps.2004.06.008

1. Introduction

Single-walled carbon nanotubes (SWNTs) are often found in self-organized bundles (Thess et al., 1996; see also López et al., 2001), i.e., a set of aligned tubes arranged in a two-dimensional triangular lattice in the plane perpendicular to their common axes. SWNT bundles have found some applications (cf. Lee et al., 2001), such as field emission electron sources for flat panel display (Baughman et al., 2002), to which both mechanical and electrical properties are important and coupled. It has been predicted (Charlier et al., 1996) that radial deformation, resulting in polygonized cross-sections, alters the band gap, leading to changes in the electron transport characteristics of carbon nanotubes. These observations have, in part, motivated a number of recent investigations to determine the linearized elastic moduli of SWNT bundles as bulk materials. Denote by x_3 the coordinate in parallel to the common axes of tubes and x_1–O–x_2 the transverse plane. The first experimental value of shear moduli of SWNT bundle with tube diameters about 1.4 nm (nanometers) was given by Salvetat et al. (1999). It is about the out-of-plane shear moduli c_{44}, with values of 0.7–6.5 GPa (±50%), estimated from the force-deflection measurements of SWNT bundles as suspended beams loaded by an atomic force microscopy (AFM). Interestingly, they have also given a theoretical but remarkably overestimated prediction 19.5 GPa. A very recent work of Lasjaunias et al. (2003) gives the estimate of the shear modulus $c_{44} = 1.1$–1.2 and 2.0 GPa for SWNT bundle samples produced by the arc discharge and laser vaporization techniques, respectively. Regarding the in-plane shear modulus c_{66}, there have only some model results, such as those by Popov et al. (2000) and Saether et al. (2003), with the predicted values 5.3 and 22.5 GPa, respectively. Saether et al. (2003) and Saether (2003) calculated the area modulus, shear modulus, Young's modulus, normal stiffness and Poisson's ratio, all within the transverse plane of a SWNT bundle, using a model in which each tube is treated as a rigid continuum tube with perfectly circular cross-section and the intertube van der Waals interaction is modeled by the Lennard–Jones potential. Their calculated values for the five in-plane moduli are self-consistent for transverse isotropy having only two independent values, as expected for a material of hexagonal symmetry (see, for instance, Hashin and Rosen, 1964; He and Zheng, 1996), but these values show significant disparities with those computed using a force-constant lattice dynamic model by Popov et al. (2000). We have noted that the earlier work of Tersoff and Ruoff (1994), using the Tersoff potential (a valence–force model) for the intratube atomic interactions and a Lennard–Jones type potential for the intertube interactions, and the work of Lu (1997), using force constants for the intratube interaction and a Lennard–Jones 6–12 potential for the intertube interaction, have both led to significantly smaller values than those obtained by Saether et al. (2003), Saether (2003) and Popov et al. (2000).

Using a valence–force model to treat the atomic interactions within each tube and the Lennard–Jones model for van der Waals interactions between tubes, Tersoff and Ruoff (1994) predicts that tubes in SWNT bundles of diameters over 2.5 nm flatten against each other under the van der Waals attraction, forming a honeycomb structure. The polygonization of cross-sections may lead to substantial changes in

their mechanical and other physical properties (Charlier et al., 1996). It is noted that tubes with different cross-sections exhibit different σ^*–π^* hybridization and correspondingly, have different electronic structures and properties (see for instance Lammert et al., 2000). Not until recently, has a high-resolution transmission electron microscopy (HRTEM) study (see for instance López et al., 2001) brought the first direct evidence, to our best knowledge, that single-walled carbon nanotubes, in bundles, with diameter as small as 1.7 nm can have polygonized cross-sections in their non-stressed states. On the other hand, there have been strong evidences from Raman (Venkateswaran et al., 1999; Peters et al., 2000) and diffraction (Tang et al., 2000; Rols et al., 2001) on structural changes of SWNT bundles in response to pressure. Venkateswaran et al. (1999) reported the variations of the radial and tangential vibrational modes versus pressure and the disappearance of the radial mode intensity under high pressure. Peters et al. (2000) reported a structural transition of SWNTs under the pressure of 1.7 GPa, basing on their observed Raman shifts. Ru (2000a) suggested a simple model based on Euler's buckling formula to explain the critical pressure of hexagonization, without taking account of van der Waals interaction. The first-principle calculations by Chan et al. (2003) show that hexagonization is a just metastable state, the energy-favored transformed shapes upon pressure are elliptical at first, and then further flattened into shape like a 400-m track under higher pressure.

Tubes in a bundle interact with each other through van der Waals forces. Plano-parallel faceting surfaces between adjacent tubes have a lower van der Waals interaction energy than that between two adjacent perfectly circular tubes, a fact that favors polygonizing. The intratube interaction energy increases, however, as the tube section distorts from the circular cross-section, opposing polygonization. This deformation energy decreases with increasing tube diameter, eventually yielding to the optimization of the intertube interaction energy, and thus lattices of hexagonal SWNTs in bundles are more stable than the lattices of the corresponding circular tubes, for tubes of large diameters. The characteristics of the lattice instability have critical implications on the elastic moduli, resulting from linearization of the elastic behavior of SWNT bundles in reference to a chosen stable state.

In the present work, we first study the instability characteristics of the lattice of SWNT bundles by analyzing the balance between the intratube atomic interactions and the intertube van der Waals interactions, using a hybrid atom/continuum (HAC) model, in which the intratube interaction energy is calculated using the molecular-dynamics-based continuum approach while the intertube interaction is modeled by a usual Lennard–Jones type potential. We present this HAC model in Section 2 and the predicted onset of polygonalization versus the tube diameter and pressure. In particular, this model predicts that tube cross-sections of a perfect lattice of SWNT bundles turn from perfectly circular to hexagonal with rounded corners, as the tube diameter increases to 2.1 nm, which is larger than 1.7 nm as observed by López et al. (2001) in their HRTEM study and smaller than 2.5 nm as predicted by Tersoff and Ruoff (1994) using an atomistic approach. We note that localized structural imperfections often promote instabilities, and we show, using an illustrative example, that a slightly perturbed lattice would result in the onset of cross-section

polygonalization of tubes with a considerably smaller diameter (1.8 nm, for this example). In Sections 3 and 4, we calculate the elastic moduli of SWNT bundles in reference to a stable configuration. Owing to their transverse isotropy, the linear elastic properties of SWNT bundles can be completely characterized by five independent elastic constants, i.e., the in-plane bulk modulus or compressibility, in-plane shear modulus, axial Young's modulus, out-of-plane Poisson's ratio and out-of-plane shear modulus. There have been a number of theoretical studies on moduli, as cited previously, but have none of these studies predicted a complete set of all five independent moduli. We predict a complete set of five moduli. We note that our estimated compressibility of 0.025 $(\text{GPa})^{-1}$ compares amazingly well with the measured value 0.024 $(\text{GPa})^{-1}$ reported by Tang et al. (2000) relatively. We also note that the deformability of tube cross-sections plays the dominant role in characterizing the transverse moduli. Interestingly, we find that the predicted elastic properties of SWNT bundles have the highest degree of anisotropy compared with those of all hexagonal crystals listed in the handbook by Every and McCurdy (1992).

2. Stability analysis

The shape of the tube cross-section of SWNT bundles results from a delicate balance between the van der Waals energy of intertube interaction and the deformation energy associated with the distortion of the intratube atomic arrangement. We assume that the lattice structure of tubes evolves, with increasing either hydrostatic pressure or tube diameter, from circular to hexagonal, through an intermediate lattice structure formed by hexagonal tubes with rounded corners, as schematically illustrated in Fig. 1. This triangular lattice (connecting the centers of

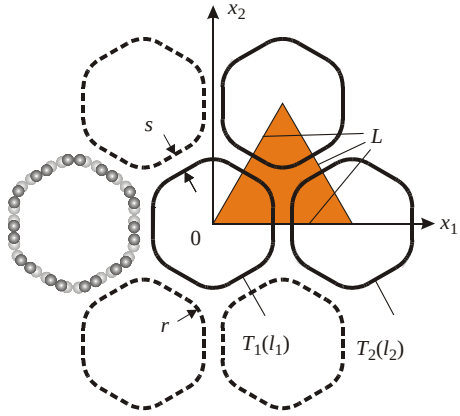

Fig. 1. A schematic illustration of a hexagonal lattice and the triangle lattice unit (the shaded portion) of SWNT bundles with the lattice constant L and intertube spacing s. The cross-section of each tube is hexagonal with rounded corners of the same radius r. T_1 and T_2 denote two adjacent tubes and l_1 and l_2, their cross-sections.

the three adjacent tubes to form a lattice unit) is characterized by the lattice constant, L, the round corner radius, r, and the effective radius[1], R, of the nearly hexagonal cross-section. In this section, we take the representative volume to be the triangular lattice unit with unit axial thickness, to study the stability of the lattice subjected to in-plane pressure.

In response to the in-plane pressure with the restriction of no axial extension, the cross-sections of SWNTs in the bundle deform through bending in the plane and contracting along the circumference. The comparison studies, see for example Yakobson et al. (1996), between MD simulations and continuum shell models have shown that SWNTs can be well modeled as super-thin shells of linear elasticity with the effective thickness[2] $t_{\text{swnt}} = 0.066\,\text{nm}$, Young's modulus $E_{\text{swnt}} = 5.5\,\text{TPa}$, and Poisson's ratio $\nu_{\text{swnt}} = 0.19$. Correspondingly, the deformation energy associated with the distortion of the intratube atomic arrangement is taken to be the sum of those associated with the bending and contracting deformation modes. For the representative volume, we have the following representations for the bending and contraction energy densities, respectively:

$$U_{\text{b}} = \frac{\pi E_{\text{swnt}} t_{\text{swnt}}^3}{24(1-\nu_{\text{swnt}})\Omega_0}\frac{1}{R}, \quad U_{\text{c}} = \frac{\pi E_{\text{swnt}} t_{\text{swnt}} R_0}{2\Omega_0}\left(\frac{R}{R_0}-1\right)^2, \tag{1}$$

where $\Omega_0 = \sqrt{3}L_0^2/4$, L_0 and R_0 are the cross-section area of the representative triangular unit, the lattice constant and the effective radius, respectively, in the absence of pressure.

We turn now to model the intertube van der Waals interaction in the usual way with a Lennard–Jones 6–12 pair potential between the ith and jth carbon atoms, located respectively on two adjacent tubes

$$\Phi_{ij} = A\left(\frac{1}{2}\frac{d_0^6}{r_{ij}^{12}} - \frac{1}{r_{ij}^6}\right), \tag{2}$$

where r_{ij} is the separation distance between the two atoms, and $A = 24.3 \times 10^{-79}\,\text{J m}^6$ and $d_0 = 0.383\,\text{nm}$ are parameterized to describe interlayer forces in graphite (see, for instance, Tersoff and Ruoff, 1994; and Girifalco et al., 2000). For each carbon atom within the representative volume, we account for its van der Waals interaction energy with all the atoms of adjacent tubes, and we then sum it over all the atoms within the representative volume and divide a half of the sum by the volume, leading to an estimate of the intertube interaction energy density U_{vdw}. Direct calculations show that interaction energies from atoms of all the non-adjacent tubes have a positive but negligible contribution[3] and are thus neglected for simplicity. To obtain an analytic representation of U_{vdw} for the convenience of the

[1]The effective radius is defined as the ratio of the circumference length of the cross-section over a fact 2π and is equal to the actual radius if the cross-section is perfectly circular.

[2]We note that there have been different opinions in the literature on the choice of the wall thickness for an equivalent continuum shell model, see Ru (2000b), and Liu et al. (2003).

[3]These contributions are 1.1%, 0.8%, 0.4%, 0.2% for tubes of diameters 1.0, 1.2, 1.6, 2.0 nm, respectively.

stability analysis, one can use an alternative approach by replacing the discrete distribution of atoms along the tube with a continuum distribution with the same atom density $\rho = 4\sqrt{3}/9a^2$, as we did in a previous work on the proposed use of multiwalled carbon nanotubes as ultrafast molecular oscillators (Zheng and Jiang, 2002; Zheng et al., 2002), where $a = 0.142\,\text{nm}$ is the carbon–carbon (C–C) bond length. We note the earlier use of a similar approach by Henrard et al. (1999) and Girifalco et al. (2000) to calculate the intertube interaction energies of carbon nanotubes and SWNT bundles. This approach leads to the following representation for the intertube interaction energy density:

$$U_{\text{vdw}} = \frac{3\rho^2}{2\Omega_0}\oint_{l_1}\int\int_{T_2}\Phi_{12}\,\mathrm{d}T_2\,\mathrm{d}l_1 = \frac{9\pi A\rho^2}{16\Omega_0}\oint_{l_1}\oint_{l_2}\left(\frac{21}{64}\frac{d_0^6}{d^{11}} - \frac{1}{d^5}\right)\mathrm{d}l_2\,\mathrm{d}l_1, \tag{3}$$

where $\oint_{l_1}\mathrm{d}l_1$ and $\oint_{l_2}\mathrm{d}l_2$ denote the integrations over the circumferences of the cross-sections of two adjacent tubes say T_1 and T_2, within the same plane perpendicular to the common axis of the tubes, $\int\int_{T_2}\mathrm{d}T_2$ denotes the area integration over the surface of the tube T_2. Φ_{12} appearing in Eq. (3) is the Lennard–Jones 6–12 potential, given in Eq. (2), between two atoms located, respectively, on l_1 and on T_2, and d denotes the distance between two atoms located on l_1 and l_2, respectively. To derive Eq. (3), we have noted that the total number of atoms on a tube section of unit axial length is equal to twice the number within one representative volume and that each tube (e.g. T_1) has 6 adjacent tubes.

We then optimize the total interaction energy density U, i.e., the sum of both the intratube and intertube interaction energy densities, for each given lattice constant L, by selecting the round corner radius, r, and the effective radius, R, of the nearly hexagonal cross-section, leading to an equilibrium state together with the corresponding total interaction energy density U^*. The equilibrium state with the lowest energy is the state with zero pressure. The in-plane strain ε, measured with respect to this state is obtained as $(L - L_0)/L_0$, in which L_0 is the lattice constant in the absence of pressure. Differentiating the total interaction energy density U^* with respect to twice of the in-plane strain ε leads to the corresponding pressure p and hence the normal stresses σ_{11} and σ_{22}

$$\sigma_{11} = \sigma_{22} = -p = \frac{1}{2}\frac{\partial U^*}{\partial \varepsilon}. \tag{4}$$

The thus obtained pressure–strain relations for SWNT bundles with tube diameters ranging from 1 to 2.1 nm are shown in Fig. 2. We note that the sharp inflection point of each pressure–strain curve, for a fixed tube diameter, corresponds to the pressure or strain at which the tube section changes from perfectly circular to hexagonal with rounded corners. For instance, the pressure–strain curve for SWNT bundles with tube diameter of 1.4 nm has a sharp inflection point near $p = 1.8\,\text{GPa}$, at which it turns from nonlinear to nearly linear with the increasing pressure, and this agrees well with the experimental observation ($p = 1.7\,\text{GPa}$) (see for instance Peters et al., 2000). A detailed examination of the lattice distortion in response to the pressure reveals that the lattice distortion prior to the inflection point is essentially due to the

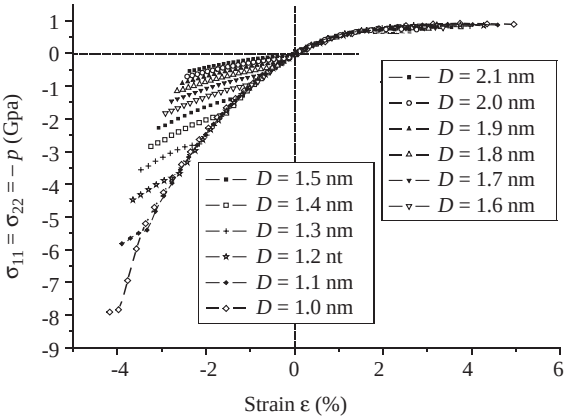

Fig. 2. The pressure–strain relations for SWNT bundles with diameters ranging from 1.0 to 2.1 nm.

shortening of the intertubular spacing, while the lattice distortion after the inflection point is dominated by the tube section change. Correspondingly, the change of the total energy is primarily attributable to the change in the van der Waals intertube interaction energy before the inflection point, and is afterwards dominated by the increase of the intratube deformation energy. This observation is consistent with the plotted pressure–strain curve, considering the fact that the Lennard–Jones 6–12 potential is highly nonlinear with respect to the interatomic distance, while the bending energy is quadratic. We have also noted that the energy contribution of the section circumferential contraction is negligibly small in comparison with that of the section wall bending.

We note the work of López et al. (2001) reporting their HRTEM observation of a lattice of polygonized tubes of section diameter 1.7 nm, approximately, in a SWNT bundle, under no externally applied pressure, and we also note the predicted larger diameters for the onset of polygonization by atomic models, such as Tersoff and Ruoff (1994) for diameters larger than 2.5 nm, in comparison with the onset diameter 2.1 nm predicted in the present work as shown in Fig. 2. It is, however, well-known that structural instabilities are often affected by local minimizers of the system energy function, which weakens the conditions for the onset of structural transition. Also, localized structural imperfections often promote instabilities. As an illustrative example, we have considered a slightly altered hexagonal lattice with the hexagonal cell comprised of one central tube of diameter 1.807 nm surrounded by six tubes of the diameter 1.797 nm yielding the mean diameter 1.800 nm. For this slightly perturbed lattice, the pressure–strain curve plotted in Fig. 3a has two inflection points, corresponding to the two discontinuous points on the tangent area modulus curve shown in Fig. 3b of the pressure–strain curve. The first one near the origin corresponds to the point where the central tube turns from perfectly circular to nearly hexagonal and the second signals the onset of polygonalization of all the surrounding tubes. This example illustrates the significant effect of apparently minor

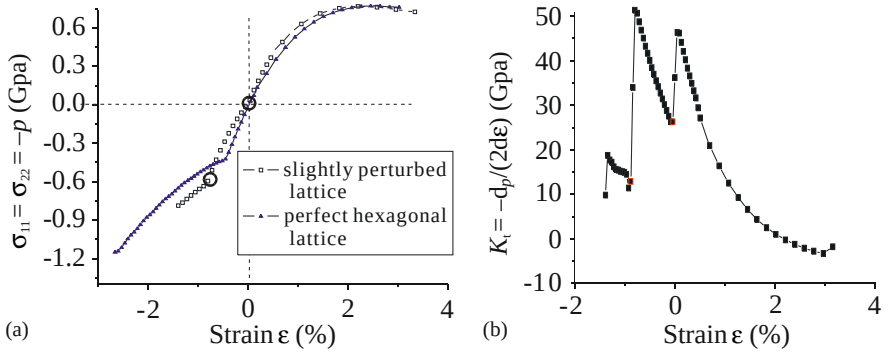

Fig. 3. The effect of a minor perturbation in the lattice upon the onset of polygonization. (a) The pressure–strain curves for the perfectly hexagonal lattice with diameter $D = 1.80$ nm and for the slightly perturbed lattice with diameter $D = 1.797,\ 1.807$ nm. (b) The tangent area modulus versus the strain for the slighted perturbed lattice.

structural imperfections upon the onset of polygonalization of tube sections. In this regard, we have noted the recent work of Saether (2003) concerning the effect of random perturbations in the lattices of SWNT bundles upon their transverse elastic moduli, using Monte Carlo simulations.

3. Transverse elastic properties of SWNT bundles

We note from Fig. 2, with surprise, that the pressure–strain curves for tubes of different diameters nearly coincide prior to their respective inflection points, and this implies that the in-plane bulk modulus (or area modulus) $K = (c_{11} + c_{12})/2$ at the origin is nearly independent of tube diameter. We have made some attempts to understand this apparent coincidence, as summarized in Appendix A. Fitting the pressure–strain curves near the origin, we obtain the area modulus $K = 40$ GPa. Considering that the axial rigidity of nanotubes is comparatively very large, we estimate the compressibility $1/K = 0.025\ (\text{GPa})^{-1}$, which is excellently consistent with the measured value $0.024\ (\text{GPa})^{-1}$ reported by Tang et al. (2000). In comparison, Tersoff and Ruoff (1994), Lu (1997), Popov et al. (2000), and Saether et al. (2003) predicted $K = 33.6,\ 18.0,\ 42.0,\ 45.8$ GPa, respectively. It is evident in Fig. 2 that the tangent area modulus, $K_t = -(1/2)\mathrm{d}p/\mathrm{d}\varepsilon$, suffers a sudden drop at the inflection point. We list in Table 1 the tangent area modulus for SWNT bundles of selected tube diameters, just after the respective inflection points, showing that the area modulus decreases significantly with the increasing tube diameter. This indicates that SWNT bundles of larger tube diameters are more compressible than those of smaller tube diameters, as expected.

In the transverse plane, the linear elastic behavior of the SWNT bundles is characterized by two independent material constants. We turn now to determine the in-plane shear modulus c_{66} by considering the pure shear deformation mode,

generated by application of tensile and compressive strain, of equal magnitude ε, along two mutually perpendicular directions of the lattice. We assume that the lattice structure of SWNTs, in the pure (double) shear deformation mode, evolves from circular to elliptic as schematically illustrated in Fig. 4. As the tube section turns into elliptic, the bending energy admits the following representation, differing from that given in Eq. $(1)_1$ for tubes of circular section:

$$U_{\mathrm{b}} = \frac{E_{\mathrm{swnt}} t_{\mathrm{swnt}}^3}{48(1-\nu_{\mathrm{swnt}}^2)\Omega_0} \oint_{l_1} \frac{\mathrm{d}l_1}{R_{\mathrm{c}}^2}, \tag{5}$$

where R_{c} is the curvature radius of the ellipse with the two primary radii R_1 and R_2. The representations for the contraction energy and the van der Waals intertube interaction energy formally remain the same as given in Eqs. $(1)_2$ and (2), respectively. For each pair of the given lattice constants $L_1 = (1-\varepsilon)L_0$ and $L_2 = \sqrt{1-\varepsilon+\varepsilon^2}L_0$, optimization of the total energy density by selecting R_1 and R_2 leads to an equilibrium state with the corresponding total interaction energy density U^*. We find that the plots of the total interaction energy density U^* versus each corresponding strain ε are quadratic, and that the energy density increases continuously with the increasing strain, as shown by an example given in Fig. 5 for such a lattice of SWNTs of tube diameter 1.4 nm. Correspondingly, the shear response, i.e., the shear stress τ versus the shear strain $\gamma = \varepsilon$, is expected to be linear, in sharp contrast to the strain response to the pressure characterized by an inflection point where the tube section turns from perfectly circular to hexagonal with rounded

Table 1
Tangent area modulus K_{t} of SWNT bundles with hexagonal cross-sections

D_0 (nm)	1.0	1.1	1.2	1.3	1.4	1.5	1.6	1.7	1.8	1.9	2.0	2.1
K_{t} (GPa)	17.7	16.8	13.6	12.5	11.8	11.2	8.02	7.66	5.92	5.80	4.80	2.38

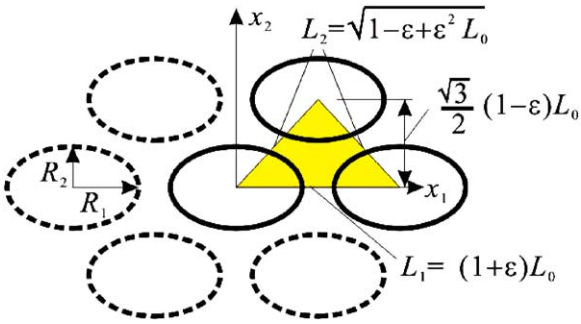

Fig. 4. A schematic illustration of the pure (double) shear deformation mode.

corners. In the shear deformation mode, the tube section turns into elliptic immediately upon loading, as illustrated by the plot of the relative radius ratio, R_2/R_0, versus the strain ε, given also in Fig. 5. Differentiating the total interaction energy density U^* with respect to the strain $\varepsilon = \gamma$ yields the shear response $\tau = \partial U^*/\partial\varepsilon = c_{66}\gamma$. The plot of the transverse (or in-plane) shear modulus c_{66} versus the tube diameter, shown in Fig. 6, indicates that the shear modulus decreases monotonically with the increasing tube diameter.

As a comparison, we reproduce the values of $c_{66} = (c_{11} - c_{12})/2$, as shown also in Fig. 6, from the plots of c_{11} and c_{12} in Fig. 1 of Popov et al. (2000). For SWNT bundles with tube diameter 0.94 nm, our predicted value $c_{66} = 2.14$ GPa is

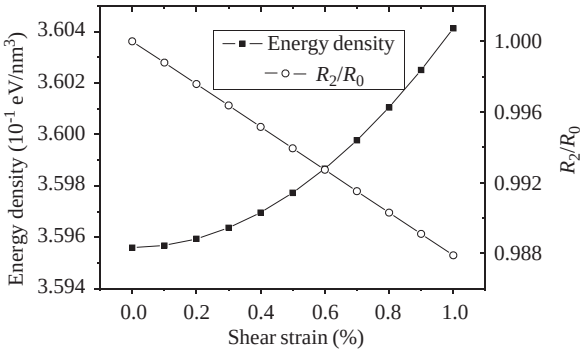

Fig. 5. The total interaction energy density U^* and the relative radius ratio R_2/R_0 versus the transverse shear strain for SWNT bundles of diameter 1.4 nm.

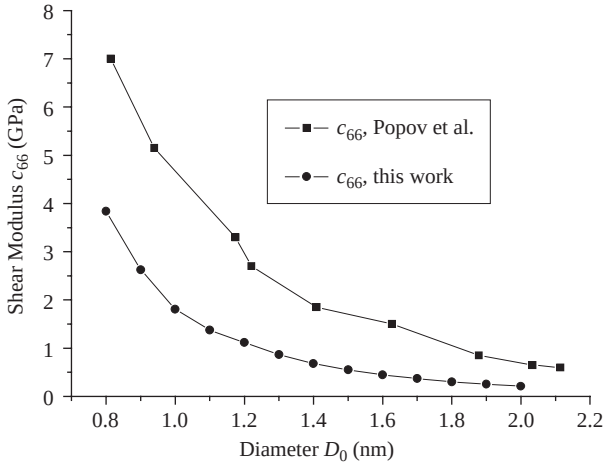

Fig. 6. The shear modulus c_{66} of SWCN bundles versus the tube diameter (in comparison with the results of Popov et al. (2000)).

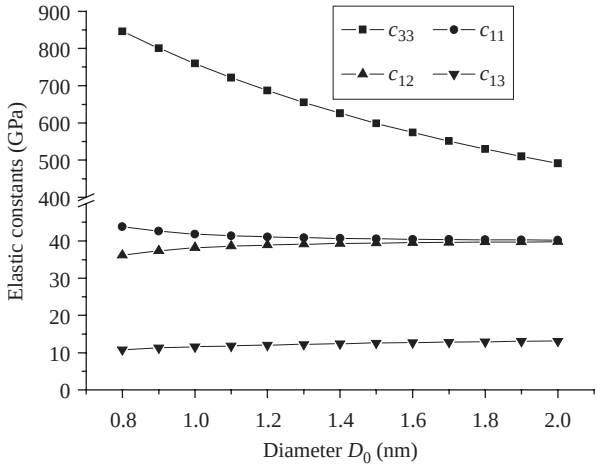

Fig. 7. The dependence of the transverse moduli c_{11}, c_{12}, c_{13} and c_{33} versus the tube diameter.

significantly smaller than the values 5.3 and 22.5 GPa estimated by Popov et al. (2000) and Saether et al. (2003), respectively. We have noted that in their works, SWNTs were treated as rigid continuum tubes with perfectly circular cross-sections. It is understandable that the assumed rigidity of the constituent tubes would render the model bulk material substantially stiffer. Since typical SWNTs bundles have tube diameters near 1.4 nm (Thess et al., 1996), comparing the two plots in Fig. 6 we see that the deformability of tube cross-sections, rather than intertube spacing changes, plays the dominant role in characterizing the transverse shear modulus. Using the relations $c_{11} = K + c_{66}$ and $c_{12} = K - c_{66}$, we further obtain the values of c_{11} and c_{12} and give their plots in Fig. 7.

Finally, we remark that in comparison with the studied tube diameter range 0.4–5.0 nm in the works of Tersoff and Ruoff (1994) and Popov et al. (2000), ours is limited to 0.8–2.1 nm, because SWNT bundles with larger tube diameters are unstable even though in the unstressed state as discussed in the previous section, and tube diameters of typical SWNT bundles have observed (Thess et al., 1996) to be about 1.4 nm.

4. The out-of-plane elastic properties of SWNT bundles

To characterize the linear elastic behavior of SWNT bundles with tube diameter smaller than the transition diameter (~ 2.1 nm for the present model) in the unstressed state, we need to determine three independent elastic moduli out of the transverse plane, in addition to the two in-plane moduli given above. Because the intertube van der Waals interaction is very weak compared with the C–C bond interaction, the axial Young's modulus, E_3, of a SWNT bundle as a bulk material

can be estimated by taking account of the contribution of C–C bonds only. This leads to

$$E_3 = \frac{\pi E_{\text{swnt}} t_{\text{swnt}} R_0}{\Omega_0} = \frac{\pi E_{\text{swnt}} t_{\text{swnt}} R_0}{\sqrt{3} L_0^2/4} = \frac{\pi E_{\text{swnt}} t_{\text{swnt}} R_0}{\sqrt{3}(2R_0 + s_0)^2/4}. \tag{6}$$

In each of the numerical studies discussed in the previous sections, the optimized intertube spacing s_0 is found to have a value very close to 3.2 nm for the tubes of diameters ranging from 0.8 to 2.1 nm, and we hence set $s_0 = 3.2$ nm. We now subject the SWNT bundle to axial strain ε_{33}, and define the Poisson's ratio $v_{13} = -\varepsilon_{11}/\varepsilon_{33}$ in terms of the transverse strain $\varepsilon_{11} = (L - L_0)/L_0$ to be calculated. We note the Poisson's ratio of SWNTs, $v_{\text{swnt}} = -(R/R_0 - 1)/\varepsilon_{33} = 0.19$, characterizing the change of radius R of a SWNT subjected to the axial strain ε_{33}. For each given axial strain ε_{33}, we optimize the intertube van der Waals interaction energy to determine the intertubular spacing s and hence the lattice constant $L = 2R + s$, and this leads to the transverse strain ε_{11} and, further, to the Poisson's ratio v_{13}. The Young's modulus E_3 and the Poisson's ratio v_{13} versus the tube diameter are both plotted in Fig. 8. The monotonic decrease of the Young's modulus is due to the fact that the atom density in the lattice decreases monotonically with the increasing tube diameter, while the Poisson's ratio is expected to increase monotonically, reaching its upper limit 0.19, the Poisson's ratio of graphite, as the diameter approaches infinity. Noting the following relations:

$$\begin{bmatrix} 1/E_1 & -v_{12}/E_1 & -v_{13}/E_3 \\ -v_{12}/E_1 & 1/E_1 & -v_{13}/E_3 \\ -v_{13}/E_3 & -v_{13}/E_3 & 1/E_3 \end{bmatrix} = \begin{bmatrix} c_{11} & c_{12} & c_{13} \\ c_{12} & c_{11} & c_{13} \\ c_{13} & c_{13} & c_{33} \end{bmatrix}^{-1} \tag{7a}$$

or their approximations because of $c_{11}, c_{12}, c_{13} \ll c_{33}$ (Popov et al., 2000)

$$E_1 \approx \frac{c_{11}^2 - c_{12}^2}{c_{11}}, \quad v_{12} \approx \frac{c_{12}}{c_{11}}, \quad E_3 \approx c_{33}, \quad v_{13} = \frac{c_{13}}{c_{11} + c_{13}} \tag{7b}$$

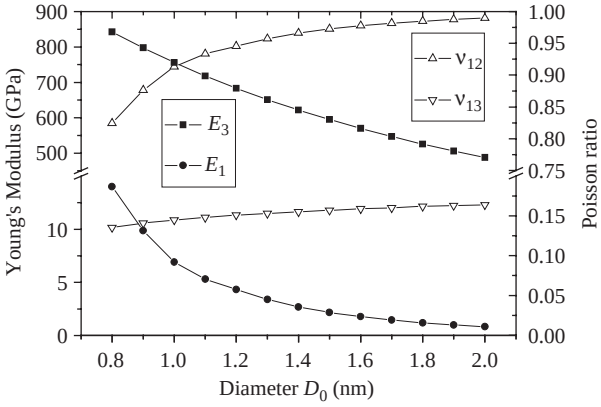

Fig. 8. The Young's moduli E_1, E_3 and Poisson's ratios v_{12}, v_{13} versus the tube diameter.

we further obtain the values of E_1, v_{12} and c_{13}, c_{33} and give their plots in Figs. 7 and 8, respectively.

Finally, we predict the out-of-plane shear modulus c_{44} ($= c_{55}$). The first estimated value of $c_{44} = 0.7$–6.5 GPa ($\pm 50\%$) was given by Salvetat et al. (1999) based on the force–deflection measurements of SWNT bundles as suspended beams loaded by an atomic force microscopy (AFM). Salvetat et al. have also given a rough model estimate 19.5 GPa. In a more recent work, with their heat capacity measurements, Lasjaunias et al. (2003) estimated the shear modulus to be $c_{44} = 1.1$–1.2 and 2.0 GPa for SWNT bundle samples produced by the arc discharge and laser vaporization techniques, respectively. We have not found more measurements of c_{44} in the literature, because the small dimensions of SWNT bundles have made it extremely difficult to measure their mechanical properties directly. The above-mentioned inconsistence between the model and experimental estimates has not been unresolved yet. Hereinafter, we propose an atomic calculation model for the estimate of c_{44}. As illustrated in Fig. 9, an out-of-plane continuum shear strain of magnitude γ corresponds to an axial slide of distance $\delta = \sqrt{3}L_0\gamma/2$, between two neighboring rows of tubes, denoted by N_1 and N_2, where L_0 is the lattice constant or the distance between the centers of two adjacent tubes. We have not found a convenient method to estimate c_{44} using the hybrid model presented in the previous sections, and we hence now turn to a purely atomic model for the estimation. We estimate c_{44} by calculating the change in the intertube van der Waals energy density U resulting from the slide and evaluating its second derivative with respect to the shear strain γ. We assume that all the tubes within one SWNT bundle have the same chirality and helical angle ϕ_0. The van der Waals interaction energy, $u(\delta, \theta_1, \theta_2)$, between two adjacent tubes, T_1 and T_2 located, respectively, on tube rows N_1 and N_2, depends upon their diameterD_0, their common helical angle ϕ_0, the slide distance δ or shear strain γ, and also upon their respective axial orientations θ_1 and θ_2 , as noted in Fig. 9. We calculate $u(\delta, \theta_1, \theta_2)$ by first computing, using the LJ potential, the interaction energy between one atom on a section of tube T_1 of length equating its axial periodicity L_P and all the atoms of tube T_2, and then summing it over all the atoms on this section of tube T_1. Since each tube, T_1, has four relatively sliding and adjacent tubes, if all these four tubes have the same axial orientation θ_2, then the changeable van der Waals interaction energy density is $u/(L_P\Omega_0)$ and the

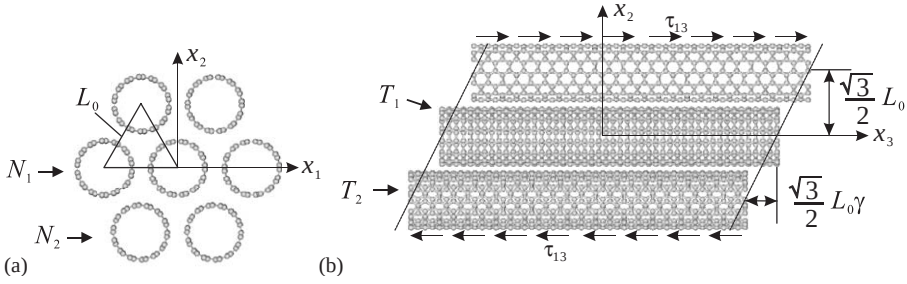

Fig. 9. A schematic illustration for the model used to estimate the out-of-plane shear modulus $c_{44} = c_{55}$.

corresponding shear modulus is thus

$$c_{44}^{\theta_1,\theta_2} = \frac{3L_0^2}{4\Omega_0 L_P} \left.\frac{\partial^2 u(\delta,\theta_1,\theta_2)}{\partial\delta^2}\right|_{\delta=\delta_{\min}}, \tag{8}$$

where $\delta = \delta_{\min}$ corresponds to the minimum of $u(\delta,\theta_1,\theta_2)$ with respect to δ. Figs. 10a and b show the topographies of $c_{44}^{\theta_1,\theta_2}$ for two SWNT bundles of the armchair-type (6,6) and (12,12), having diameters 0.814 and 1.62 nm, respectively. In real cases, orientations of SWNTs should correspond to a minimum of the total intertube van der Waals energy, and may have a complicated dependence upon both the diameter D_0 and charity ϕ_0. Nevertheless, we have the following upper and lower bounds:

$$c_{44}^{\min} = \min_{\theta_1,\theta_2} c_{44}^{\theta_1,\theta_2} \leqslant c_{44} \leqslant c_{44}^{\max} = \max_{\theta_1,\theta_2} c_{44}^{\theta_1,\theta_2} \tag{9}$$

for the out-of-plane shear modulus c_{44}. In the above analysis, we have assumed that the tubes are rigid, and we have estimated that the relative error resulted from this assumption is generally less than 10%. The detailed analysis is given in Appendix B.

Recent experimental observations (Thess et al., 1996; Terrones et al., 1997) show that SWNTs, as long as about 0.1 mm, are mostly armchair tubes, although there has been an early report on the observation of chiral nanotubes (Iijima and Ichihashi, 1993). In Fig. 10c we plot these bounds for armchair SWNT bundeles of the (6,6), (8,8), (10,10), (12,12), and (14,14) tubes. Interestingly, the upper and lower bounds are almost independent of the diameter, with the values ~ 2.2 and 0.25 GPa, respectively; and their average value, 1.22 GPa, is consistent with the latest experimental estimate $c_{44} = 1.1$–1.2 GPa by Lasjaunias et al. (2003) for SWNT bundles produced by the arc discharge technique.

In summary, for typical SWNT bundles of tube diameter 1.4 nm, the predicted elastic coefficients are $c_{11} = 40.68$ GPa, $c_{12} = 39.32$ GPa, $c_{66} = (c_{11} - c_{12})/2 = 0.68$ GPa, $c_{13} = 12.40$ GPa, $c_{33} = 625.72$ GPa, and (in average) $c_{44} = 1.22$ GPa.

5. Concluding remarks

We have presented a hybrid atom/continuum (HAC) model to study the nonlinear elastic properties of SWNTs bundles as bulk materials. The main findings or new results are summarized below:

(1) The in-plane pressure–strain relations as shown in Fig. 2 for various tube diameters are given for the first time. Each exhibits a sharp inflection point, corresponding to the transition from perfectly circular to hexagonal tube cross-sections, and strong nonlinearity. This implies that the linear elastic moduli, resulting from linearization of these significantly nonlinear relations, are sensitive to the choice of reference configurations, which may or may not be the unstressed state, and that they are affected by tube diameters.

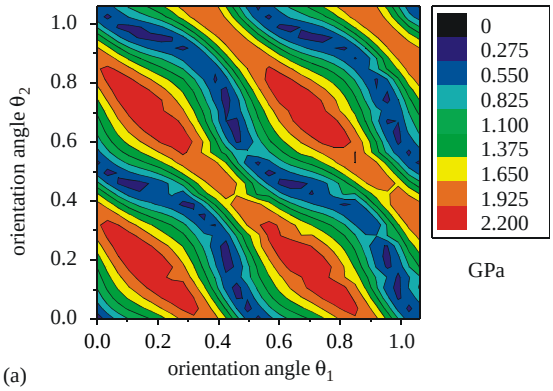

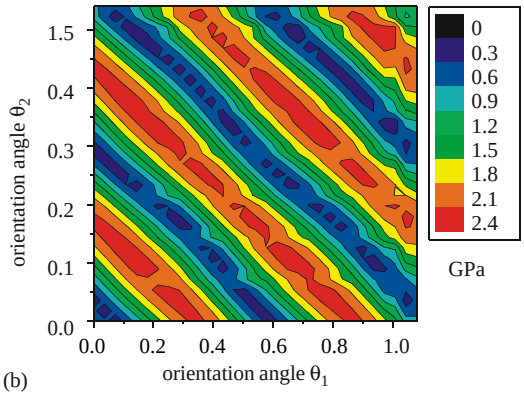

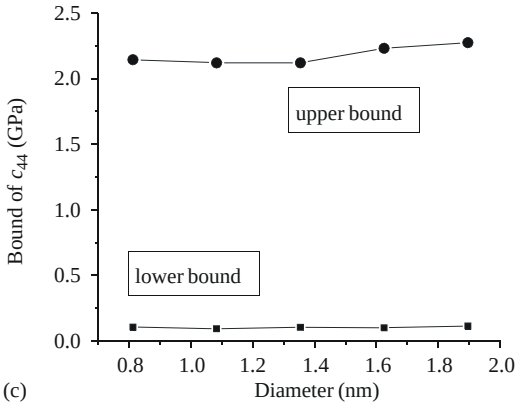

Fig. 10. The transverse shear modulus c_{44}. (a) and (b) are the topographics of the shear modulus $c_{44}^{\theta_1,\theta_2}$ depending on the orientations θ_1, θ_2 for SWNT bundles of (6,6) and (12,12) types. (c) The upper and lower bounds of c_{44}.

(2) Fig. 2 also shows that the in-plane pressure–strain relations for tubes of different diameters are of no significant difference prior to their respective inflection points, and this implies that the in-plane bulk modulus (or the area modulus) with respect to the unstressed configuration is nearly independent of tube diameter.
(3) Our predicted critical transition diameter, 2.1 nm, in the unstressed state for perfectly crystalline SWNT bundles is larger than 1.7 nm observed by López et al. (2001) in their HRTEM study and smaller than 2.5 nm as predicted by Tersoff and Ruoff (1994). We show, by an example, that imperfections in the lattice can reduce this critical value significantly (to 1.8 nm).
(4) There have been a number of theoretical studies on the linear elastic properties of SWNT bundles, but have none of these studies predicted or estimated a complete set of five independent moduli. In this work, we have predicted the in-plane bulk modulus, in-plane shear modulus, axial Young's modulus, out-of-plane Poisson's ratio, and we have obtained upper and lower bounds of the out-of-plane shear modulus. These predictions and estimates are compared well with limited measurements available in the literature.
(5) As a comparison, we have examined the elastic coefficients of all the over two hundreds hexagonal crystals listed in the handbook by Every and McCurdy (1992). It is found that the elastic properties of graphite have the highest anisotropy degree [4], 0.666, and the lowest modulus ratio, 0.39%, compared with those of all other hexagonal crystals. Interestingly, we further find that the predicted elastic properties of SWNT bundles have higher anisotropy degrees and lower modulus ratios than those of graphite. For instance, for SWNT bundles of tube diameter 1.4 nm, the anisotropy degree is 0.836, and the smallest modulus ratio is 0.11%.

Acknowledgements

We gratefully acknowledge the support of the Chinese National Natural Foundation through the Grants No. 10172051, No. 10252001, No. 10332020, and No. 10210401228, the 973-Project No. G2003CB615600, the Ministry of Education of China and her key grant project (0306), and the U.S. National Science Foundation through Grant No. CMS-0140568.

Appendix A

We have noted that simulated pressure-strain curves for SWNT bundles of different tube diameters shown in Fig. 2 nearly coincide prior to their respective

[4]The anisotropy degree is defined as $\|\mathbf{C}-\mathbf{C}_{\text{iso}}\|/\|\mathbf{C}\|$, where $\mathbf{C}$ is the elastic stiffness tensor, $\mathbf{C}_{\text{iso}}$ is the isotropic part of $\mathbf{C}$, and $\|\bullet\|$ is the standard norm.

inflection points, and this implies that the corresponding in-plane area modulus exhibits negligible dependence upon the tube diameter. We consider this observation particularly interesting, noting that the atom density of SWNT bundles is proportional to $D_0/(D_0+s_0)^2$ and thus decreases rapidly with the increasing tube diameter D_0 because the intertubular spacing s_0 for D_0 ranging from 1 to 2 nm is known to vary slightly around 3.2 nm. With this curiousness, we estimate in the following the area modulus of a SWNT bundle by modeling it as a fiber-reinforced composite material for which the mechanical properties of the effective matrix and the effective solid reinforcement fibers are characterized, respectively, by the intertube van der Waals interactions and the response of the constitutive SWNTs. For simplicity, we neglect the dependence of the in-plane area modulus of the effective matrix upon the tube diameter, considering the fact that the intertubular spacing, which is the dominating parameter in the van der Waals interaction, is known to vary very little. Thus, the diameter-dependence of the in-plane pressure–strain response properties of the composite is determined by the corresponding dependence of the in-plane effective bulk modulus K_i of the effective fibers and their volume fraction β in the composite. A simple analysis leads to the representation $K_{\mathrm{i}} = E_{\mathrm{swnt}} t_{\mathrm{swnt}}/D_0$. The volume fraction of the reinforcing component is given as below

$$\beta = \frac{\pi D_0^2/8}{\sqrt{3}(D_0+s_0)^2/4} = \frac{\pi}{2\sqrt{3}(1+s_0/D_0)^2}. \tag{10}$$

It is known from micromechanics that the stiffness of a fiber-reinforced composite increases with increasing fiber stiffness and with increasing fibre-volume fraction, provided that the fiber is stiffer than the matrix. Because of the much stronger carbon–carbon bond than that of the van der Waals interaction, the in-plane

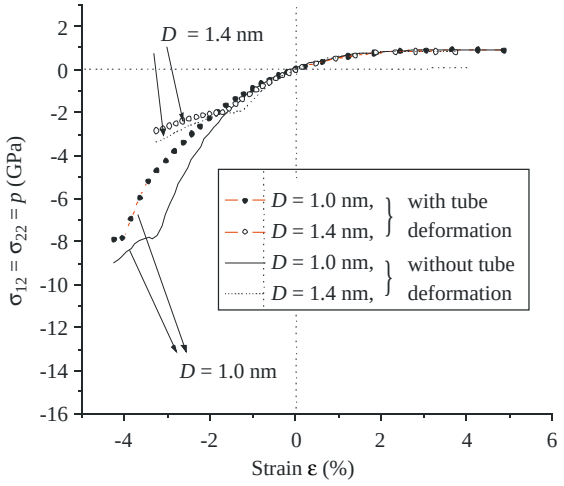

Fig. 11. The effect of tube deformations on the pressure–strain relation.

effective bulk modulus K_i for diameter D_0 smaller than 2.0 nm is larger than that of the effective matrix. Thus, an increase in the tube diameter would soften the composite through a resulting decrease in the in-plane bulk modulus K_i but stiffen the composite through the increased volume fraction β. It is therefore not unreasonable that the in-plane pressure–strain response of the composite happens to be nearly independent of the tube diameter. Physically, the tube in-plane stiffness affects the in-plane stiffness of the SWNT bundle through deformations in tube sections. To illustrate this effect, we plot in Fig. 11 the pressure–strain curves for SWNT bundles for both cases when section deformations are allowed and disallowed, and it is seen that the section deformation, and hence the tube in-plane stiffness, has a significant effect on the in-plane modulus of SWNT bundles.

Appendix B

We consider the effect of cross-section wrapping of tubes upon our estimate of the off-plane shear modulus c_{44}. In response to an applied out-of-plane shear stress τ_{23}, the intertube van der Waals interaction results in axial forces, whose distribution on a tube surface is antisymmetric with respect to the middle plane of the tube, parallel to the 1–3 plane, as illustrated in Fig. 12a, and we denote by f_{vdw} the measure of these forces per unit area on tube surfaces. Because of periodicity of the hexagonal crystalline tube arrangement, the resultant forces per unit axial length on the upper and lower semi-surfaces of each tube have equal magnitude $\tau_{23}L_0$ but opposite directions, where L_0 is the lattice constant as noted in the main text. As illustrated in Fig. 12b for the cross-section, these distributed forces are balanced by the in-shell shear stress $\tau(\varphi)$. The corresponding in-shell shear strain is $\gamma_{swnt} = \tau(\varphi)/G_{swnt}$, and for an infinitesimal circumferential segment $R_0 d\varphi$, the corresponding infinitesimal wrapping axial distance is $\gamma_{swnt} R_0 d\varphi$, where $G_{swnt} = E_{swnt}/[2(1 + \nu_{swnt})] = 231$ GPa, is the shear modulus of SWNTs as shear. Thus, the total wrapping distance for the entire tube section is given as the following:

$$\delta_w = \int_{-\pi/2}^{\pi/2} \frac{\tau(\varphi)}{G_{swnt}} R_0 \, d\varphi \tag{11}$$

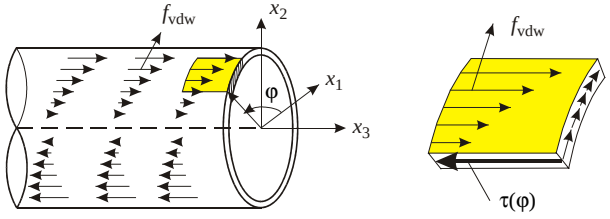

Fig. 12. A schematic illustration for the model used to account the wrapping effect.

Noting that $\tau(\varphi)$ vanishes at $\varphi = \pm\pi/2$ and reaches the extreme values at $\varphi = 0, \pi$ with the magnitude $\tau_{\max} = \tau_{23}L_0/(2t_{\text{swnt}})$, we approximate the shear stress distribution by $\tau(\varphi) = \tau_{\max}\cos\varphi$ and thus have

$$\delta_{\text{w}} = \frac{2R_0\tau_{\max}}{G_{\text{swnt}}} = \frac{R_0L_0}{G_{\text{swnt}}}t_{\text{swnt}}\,\tau_{23}. \tag{12}$$

On the other hand, by omitting the tube wrapping the intertube sliding δ can be associated with the applied shear stress τ_{23} in the form $\delta = \sqrt{3}\tau_{23}L_0/(2c_{44})$, where c_{44} ($0.25 \leqslant c_{44} \leqslant 2.2$ GPa) is the out-of-plane shear modulus estimated in Section 4 by omitting the wrapping effect. Therefore, in the presence of both intertube sliding δ and intratube wrapping δ_{w}, the bulk shear strain is given by $\gamma = 2(\delta + \delta_{\text{w}})/(\sqrt{3}L_0)$ and the shear modulus is defined as $c_{44}^* = \tau_{44}/\gamma$. These analyses yield the following relation:

$$\frac{c_{44}^*}{c_{44}} = \frac{d}{d + d_{\text{w}}} = \left(1 + \frac{D_0c_{44}}{\sqrt{3}G_{\text{swnt}}t_{\text{swnt}}}\right)^{-1}. \tag{13}$$

Finally, substituting the values of G_{swnt}, t_{swnt}, $c_{44} = 0.25$–2.2 GPa, and $D_0 = 1$–2 nm, we obtain $0.86 \leqslant c_{44}^*/c_{44} \leqslant 0.99$.

References

Baughman, R.H., Zakhidov, A.A., de Heer, W.A., 2002. Carbon nanotubes—the route toward applications. Science 297, 787–792.

Chan, S.-P., Yim, W.-L., Gong, X.G., Liu, Z.-F., 2003. Carbon nanotube bundles under high pressure: transformation to low-symmetry structures. Phys. Rev. B 68, 075404.

Charlier, J.-C., Lambin, Ph., Ebbesen, T.W., 1996. Electronic properties of carbon nanotubes with polygonized cross-sections. Phys. Rev. B 54, R8377–R8380.

Every, A.G., McCurdy, A.K., 1992. Low frequency properties of dielectric crystals. In: Nelson, D.F. (Ed.), Numerical Data and Functional Relationships in Science and Technology. Group III: Crystal and Solid State Physics. Springer, Berlin.

Girifalco, L.A., Hodak, M., Lee, R.S., 2000. Carbon nanotubes, buckyballs, ropes, and a universal graphitic potential. Phys. Rev. B 62, 13104–13110.

Hashin, Z., Rosen, B.W., 1964. The elastic moduli of fiber-reinforced materials. J. Appl. Mech. 31, 223–232.

He, Q.-C., Zheng, Q.-S., 1996. On symmetries of 2D elastic and hyperelastic tensors. J. Elasticity 43, 203–225.

Henrard, L., Hernandez, E., Bernier, P., Rubio, A., 1999. Van der Waals interaction in nanotube bundles: consequences on vibrational modes. Phys. Rev. B 60, R8521–R8524.

Iijima, S., Ichihashi, T., 1993. Single-shell carbon nanotubes of 1-nm diameter. Nature 363, 603–605.

Lammert, P.E., Zhang, P., Crespi, V.H., 2000. Gapping by squashing: metal–insulator and insulator–metal transitions in collapsed carbon nanotubes. Phys. Rev. Lett. 84, 2453–2456.

Lasjaunias, J.C., Biljackovic, K., Monceau, P., Sauvajol, J.L., 2003. Low-energy vibrational excitations in carbon nanotubes studied by heat capacity. Nanotechnology 14, 998–1003.

Lee, N.S., Chung, D.S., Han, I.T., et al., 2001. Application of carbon nanotubes to field emission displays. Diam. Relat. Mater. 10, 265–270.

Liu, J.Z., Zheng, Q.-S., Jiang, Q., 2003. Effect of bending instabilities on the measurements of mechanical properties of multiwalled carbon nanotubes. Phys. Rev. B 67, 075414.

López, M.J., Rubio, A., Alonso, J.A., Qin, L.-C., Iijima, S., 2001. Novel polygonized single-wall carbon nanotube bundles. Phys. Rev. Lett. 86, 3056–3059.

Lu, J.P., 1997. Elastic properties of carbon nanotubes and nanoropes. Phys. Rev. Lett. 79, 1297–1300.
Peters, M.J., McNeil, L.E., Lu, J.P., Kahn, D., 2000. Structural phase transition in carbon nanotube bundles under pressure. Phys. Rev. B 61, 5939–5944.
Popov, V.N., Van Doren, V.E., Balkanski, M., 2000. Elastic properties of crystals of single-walled carbon nanotubes. Solid State Commun. 114, 395–399.
Rols, S., Goncharenko, I.N., Almairac, R., Sauvajol, J.L., Mirebeau, I., 2001. Polygonization of single-wall carbon nanotube bundles under high pressure. Phys. Rev. B 64, 153401.
Ru, C.Q., 2000a. Elastic buckling of single-walled carbon nanotube ropes under high pressure. Phys. Rev. B 62, 10405–10408.
Ru, C.Q., 2000b. Effective bending stiffness of carbon nanotubes. Phys. Rev. B 62, 9973–9976.
Saether, E., 2003. Transverse mechanical properties of single-walled carbon nanotube crystals Part II: sensitivity to lattice distortion. Comput. Sci. Technol. 63, 1551–1559.
Saether, E., Frankland, S.J.V., Pipes, R.B., 2003. Transverse mechanical properties of single-walled carbon nanotube crystals Part I: determination of elastic moduli. Comput. Sci. Technol. 63, 1543–1550.
Salvetat, J.-P., Briggs, G.A.D., Bonard, J.-M., Bacsa, R.R., Kulik, A.J., Stöckli, T., Burnham, N.A., Forró, L., 1999. Elastic and shear moduli of single-walled carbon nanotube ropes. Phys. Rev. Lett. 82, 944–947.
Tang, J., Qin, L.C., Sasaki, T., Yudasaka, M., Matsushita, A., Iijima, S., 2000. Compressibility and polygonization of single-walled carbon nanotubes under hydrostatic pressure. Phys. Rev. Lett. 85, 1887–1889.
Terrones, M., Grobert, N., Olivares, J., Zhang, J.P., Terrones, H., Kordatos, K., Hsu, W.K., Hare, J.P., Townsend, P.D., Prassides, K., Cheetham, A.K., Kroto, H.W., Walton, D.R.M., 1997. Controlled production of aligned-nanotube bundles. Nature 388, 52–55.
Tersoff, J., Ruoff, R.S., 1994. Structural properties of a carbon-nanotube crystal. Phys. Rev. Lett. 73, 676–679.
Thess, A., Lee, R., Nikolaev, P., Dai, H.J., Petit, P., Robert, J., et al., 1996. Crystalline ropes of metallic carbon nanotubes. Science 273, 483–487.
Venkateswaran, U.D., Rao, A.M., Richter, E., Menon, M., Rinzler, A., Smalley, R.E., Eklund, P.C., 1999. Probing the single-wall carbon nanotube bundle: Raman scattering under high pressure. Phys. Rev. B 59, 10928–10934.
Yakobson, B.I., Brabec, C.J., Bernholc, J., 1996. Nanomechanics of carbon tubes: instability beyond linear response. Phys. Rev. Lett. 76, 2511–2514.
Zheng, Q.-S., Jiang, Q., 2002. Multiwalled carbon nanotubes as gigahertz oscillators. Phys. Rev. Lett. 88, 045503.
Zheng, Q.-S., Liu, J.Z., Jiang, Q., 2002. Excess van der Waals interaction energy of a multiwalled carbon nanotube with an extruded core and the induced core oscillation. Phys. Rev. B 65, 245409.